Mechanism of hydrogen on cervical cancer suppression revealed by high-throughput RNA sequencing

JING CHU*, JINGHAI GAO*, JING WANG, LINGLING LI, GUOQIANG CHEN,
JIANHONG DANG, ZHIFENG WANG, ZHIJUN JIN and XIAOJUN LIU

Department of Obstetrics and Gynaecology, Changzheng Hospital, Naval Medical University, Shanghai 200003, P.R. China

Abstract. Cervical cancer is considered one of the diseases with the highest mortality among women and with limited treatment options. Hydrogen (H_2) inhalation has been reported to have a variety of tumor-suppressive effects, but the exact mechanism remains unclear. In the present study, HeLa cervical cancer cells and HaCaT keratinocytes treated with H_2, and a HeLa xenograft mouse model subjected to H_2 inhalation were established. TUNEL, Cell Counting Kit-8 and Ki67 staining assays were used to detect cell apoptosis and proliferation. Oxidative stress was determined according to the levels of reactive oxygen species, malondialdehyde and superoxide dismutase. Tumor growth was recorded every 3 days, and the excised tumors were stained with hematoxylin and eosin. High-throughput RNA sequencing and subsequent Gene Ontology (GO) enrichment analysis were performed in HeLa-treated and un-treated HeLa cells. The expression of hypoxia-inducible factor (HIF)-1α and NF-κB p65 was verified by western blotting, immunohistochemistry and reverse transcription-quantitative PCR. The results revealed an increased apoptosis rate, and reduced cell proliferation and oxidative stress in H_2-treated HeLa cells but not in HaCaT cells. Similarly, decreased tumor growth and cell proliferation, and enhanced cell apoptosis were observed in H_2-treated HeLa tumors. RNA sequencing and GO analysis suggest that downregulated *HIF1A* (HIF-1α mRNA) and *RelA* (NF-κB p65) levels, and reduced NF-κB signaling were associated with the antitumor effect of H_2. Finally, decreased HIF-1α and NF-κB p65 expression both at the transcriptional and translational levels were observed in H_2-treated HeLa cells and in HeLa-derived tumors. In conclusion, the present study reveals a novel mechanism of H_2 against cervical cancer, which may serve as a potential therapeutic target in clinical practice.

Introduction

Cervical cancer is the fourth most common type of cancer and the fourth leading cause of cancer-associated mortality among women worldwide (1). In addition, cervical cancer is the second leading cause of cancer-associated mortality in women aged 20-39 years in the USA, and it was estimated that there may be 13,800 new cases and 4,290 mortalities in 2020 (2). Radical hysterectomy with pelvic lymphadenectomy is the standard recommended surgical therapy for patients with early-stage cervical cancer (3). However, this method also increases the number of circulating tumor cells, and promotes cancer progression and metastasis (4). In addition to surgical therapy, molecular-targeted strategies have recently received attention in the field of cancer treatment. However, molecular-targeted strategies have not shown significant benefit in the majority of patients with cervical cancer, as these precision drugs are available for only 3-13% of patients (5,6). Thus, alternative treatments for patients with cervical cancer are needed.

Molecular hydrogen (H_2) biology and H_2 therapy are novel and rapidly developing areas of research (7-9). H_2 has been shown to exert antioxidant and anti-inflammatory effects (10), and to protect neurons from oxidative stress injury during cerebral ischemia-reperfusion (11). Importantly, since the tumorigenesis and progression of cancer are closely associated with the levels of peroxidation and inflammation, H_2 may play a role in tumor regulation in endometrial (12), lung (13) and breast cancer (14). A prospective follow-up study of 82 patients with stage III and IV cancer, including lung, pancreatic and gynecological cancer (including cervical cancer), revealed significant improvements in fatigue, insomnia, anorexia, pain and physical status after 4 weeks of H_2 inhalation (15). However, the potential antitumor mechanism of H_2 intervention in cervical cancer is currently unknown.

High-throughput RNA sequencing is a powerful method for revealing transcriptional and non-transcriptional signatures in cells and animals (16). It maximizes the identification of the regulatory effects of different treatments at the genetic level. The human cervical adenocarcinoma HeLa cell line expresses

Correspondence to: Professor Zhijun Jin or Professor Xiaojun Liu, Department of Obstetrics and Gynaecology, Changzheng Hospital, Naval Medical University, 415 Fengyang Road, Shanghai 200003, P.R. China
E-mail: j_zj888@163.com
E-mail: liuxiaojun@smmu.edu.cn

*Contributed equally

over 10,000 proteins and is considered the most commonly analyzed cells in cervical cancer research (17,18). Previous studies reported that HeLa cells can be used *in vitro* (19) and in *in vivo* xenotransplant models (20) to simulate the process of cervical cancer. In addition, HeLa cells have been used to investigate the regulatory role of H_2 in Wnt/β-catenin signaling (21). But the tumor inhibitory effect of H_2 and its related mechanism in HeLa cells remain unknown. Thus, RNA sequencing of control and H_2-treated HeLa cells may be helpful for identifying the potential antitumor mechanism of H_2 in cervical cancer.

The present study demonstrated that treatment with 66.7% H_2 significantly elevated the apoptosis rate, and reduced the cell proliferation and oxidative stress of HeLa cells *in vitro*. Furthermore, tumor growth and cell death were also observed in H_2-treated HeLa tumors. Decreased hypoxia inducible factor (*HIF)1A* and RELA proto-oncogene, NF-κB subunit (*RelA*) expression levels were detected in the H_2 group through RNA sequencing. The expression of *HIF1A* and *RelA* and their encoded protein expression were further confirmed by reverse transcription-quantitative PCR (RT-qPCR), western blotting, and immunohistochemistry (IHC).

Materials and methods

Cell line and cell experiments. The human cervical cancer HeLa cell line and nontumor HaCaT keratinocytes were purchased from the American Type Culture Collection. Cells were cultured in DMEM (Gibco; Thermo Fisher Scientific, Inc.) supplemented with 10% filtered FBS (Gibco; Thermo Fisher Scientific, Inc.) at 37°C in a humidified 5% CO_2/95% air environment. For H_2 intervention, H_2 gas was produced by a H_2-O_2 nebulizer (AMS-H-01; Asclepius), and HeLa and HaCaT cells were incubated at 37°C in a mixture of 33.3% H_2/33.3% N_2/33.4% O_2 or 66.7% H_2/33.3% O_2 environment for 1 h every 12 h. Cisplatin was obtained from APeXBIO Technology LLC (cat. no. A8321). Our preliminary results suggested that the IC_{50} of cisplatin treatment of HeLa cells for 24 h is 12 μg/ml, which is consistent with previously reported results (22). Cisplatin was used in the present study at a concentration of 5 μg/ml. After 7 days of H_2 treatment, cells were evaluated for their viability, apoptosis, reactive oxygen species (ROS), malondialdehyde (MDA) and superoxide dismutase (SOD) levels. In addition, RNA was isolated for RNA sequencing. Cells cultured under a normal environment were used as control.

Animal experiments. A total of 22 female athymic BALB/c nude mice (age, 5-6 weeks old; weight, 20-25 g) were obtained from Jackson Laboratory and housed in a pathogen-free facility with temperature of 18-29°C, relative humidity of 40-70%, 12-h light/dark cycle, and free access to food and water. HeLa cells ($1x10^7$ cells in 200 μl PBS) were subcutaneously injected into the left armpit of nude mice. Tumor-bearing mice were monitored by body condition scoring index and clinical evaluations every day, and were euthanized by administration of an overdose of pentobarbital sodium (100 mg/kg) if they exhibited either a >10% decrease in body weight compared with pre-injection body weight or if their activity level declined due to tumor burden. In total, 4 tumor-bearing mice were

euthanized who reached the aforementioned humane endpoints. At 7 days post-injection, the remaining tumor-bearing mice were randomly divided into two groups: The group housed under normal conditions (control group, n=9) and the H_2 intervention group (H_2 group, n=9). To establish a H_2 intervention model, mice were kept in a mixture of 66.7% H_2/33.3% O_2 environment for 30 min per day (11), and after 27 days, the mice were sacrificed with 100 mg/kg pentobarbital sodium as evidenced by the disappearance of breathing and heartbeat to collect the tumors. Tumor volumes were estimated as the length x width^2 x 0.5 every 3 days starting from 7 days after cell injection. The maximum tumor volume observed in the present study was 1,582 mm^3. All animal experiments were performed in accordance with the National Institutes of Health (NIH) Guide for the Care and Use of Laboratory Animals, and were approved by the Ethics Committee for Animal Studies of Naval Medical University (approval no. 202027).

Cellular apoptosis and proliferation assay. TUNEL assay by immunofluorescence staining was performed to determine the cellular apoptosis rate. Briefly, $2x10^4$ HeLa or HaCaT cells were seeded into 48-well plates and, after H_2 intervention, the cells were fixed with 4% paraformaldehyde for 10 min at room temperature. After permeabilization with 0.1% Triton X-100 (Sigma-Aldrich; Merck KGaA) for 10 min at room temperature, the cells were blocked with 5% BSA (Sigma-Aldrich; Merck KGaA) for 10 min at room temperature. Furthermore, the *In situ* Cell Death Detection kit (cat. no. 11684809910; Roche Diagnostics) was used according to the manufacturer's protocol, and cells were then counterstained with DAPI (Sigma-Aldrich; Merck KGaA) for nuclear staining and observed through a fluorescence microscope (Olympus Corporation). The percentage of TUNEL-positive cells was calculated as the ratio of the number of TUNEL-positive nuclei/total number of nuclei, which were counted in three different random fields of view. Cell proliferation was evaluated using a Cell Counting Kit (CCK)-8 assay (cat. no. C0037; Beyotime Institute of Biotechnology) following the manufacturer's instructions. The absorbance at 450 nm was detected using a microplate reader (BioTek Instruments, Inc.).

Cellular oxidative stress detection. The level of ROS was determined using the Cellular ROS Assay kit (cat. no. ab113851; Abcam) according to the manufacturer's instructions. The ROS level was calculated as ROS positive area/total area x 100%. In addition, MDA and SOD levels were detected using the commercially available test kits Lipid Peroxidation (MDA) Assay kit (cat. no. ab118970; Abcam) and SOD Colorimetric Activity kit (cat. no. EIASODC; Invitrogen; Thermo Fisher Scientific, Inc.) according to the manufacturer's protocol.

Hematoxylin and eosin (H&E) staining and immuno-histochemistry (IHC). HeLa tumors fixed in 4% paraformaldehyde were dehydrated and then embedded in paraffin. Next, samples were sectioned at 5-μm thickness and stained with hematoxylin and eosin (H&E). Tumor histopathological changes were captured with an optical microscope (Olympus Corporation).

For IHC, the sections were deparaffinized, hydrated at 70°C in xylene and microwaved at full power for 20 min for

antigen retrieval using sodium citrate (pH 6.0). In addition, 5% BSA was used as the blocking reagent overnight at 4˚C. Next, the slides were incubated with anti-HIF-1α primary antibody (1:100; cat. no. ab51608; Abcam), anti-NF-κB p65 primary antibody (1:200; cat. no. ab16502; Abcam) or anti-Ki67 primary antibody (1:200; cat. no. ab15580; Abcam) overnight at 4˚C. The next day, the slides were washed three times with PBS and incubated with a goat anti-rabbit polyclonal HRP-conjugated secondary antibody (1:50; cat. no. 32260; Thermo Fisher Scientific, Inc.) for 2 h at room temperature. After diamino-benzidine staining (Invitrogen; Thermo Fisher Scientific, Inc.), images were captured with an optical microscope and analyzed using ImageJ 1.53 software (NIH). TUNEL assay by IHC was performed with DeadEnd™ Colorimetric TUNEL system (cat. no. G7360; Promega Corporation) according to the manufacturer's instructions.

RNA sequencing. cDNA libraries were constructed in a strand-specific manner from 4 μg DNase-treated RNA using TruSeq Stranded Total RNA Library Prep kit (cat. no. 20020597; Illumina, Inc.). Total RNA, including mRNA and small RNA (circRNA, lncRNA, and miRNA) was then fragmented, subjected to two rounds of cDNA synthesis, and adapters were then ligated to double-strand cDNA. All libraries were sequenced on Illumina NovaSeq 6000 and HiSeq X Ten platforms (Illumina, Inc.), generating 100-bp paired-end reads. High-quality reads were obtained by trimming adapter sequences, invalid and low-quality reads from the raw reads (quality control). The clean reads were then mapped to the human genome by HISAT2 software (v 2.1.0) using default parameters. Next, transcript assemblies were constructed using StringTie software (v 1.3.6; The Center for Computational Biology at Johns Hopkins University) to merge transcripts, and DESeq2 software (v 2.11.40.2; Bioconductor, Inc.) was used to compute differential expression.

Bioinformatic analyses. Multivariate analysis and principal component analysis were performed by ClustVis online tool (https://github.com/fw1121/ClustVis) (23). Gene Ontology (GO) enrichment analysis was carried out using DAVID bioinformatics tool (https://david.ncifcrf.gov/tools.jsp) (24). A hypergeometric test (Fisher's exact test) was used to calculate the statistical significance of gene overrepresentation, followed by a Bonferroni correction for multiple comparisons to estimate the proportion of enriched genes that may occur by chance for the given set of genes. Heatmaps and volcano plots were generated using TBtools (v 1.055; programmed by C.J. Chen). Fold-change (FC) was calculated as the mean value of RNA reads in H_2 groups/mean value in controls.

Western blotting. Protein samples from HeLa cells in the control and H_2 treatment groups were lysed with Tissue or Cell Total Protein Extraction kit (cat. no. C510003; Sangon Biotech Co., Ltd.) following the manufacturer's protocol. Protein concentration was determined using a BCA Protein Assay kit (cat. no. P0010; Beyotime Institute of Biotechnology). Equal quantities of protein (20 μg per lane) from the lysate of control or H_2 treatment groups were subjected to SDS-PAGE. After transferring to a PVDF membrane and blocking with 5% skimmed milk for 2 h at room temperature, the membrane was

incubated overnight at 4˚C with specific primary antibodies against HIF-1α (cat. no. ab51608), GAPDH (cat. no. ab8245), NF-κB (cat. no. ab16502) or lamin B1 (cat. no. ab16048) (all from Abcam) at a 1:1,000 dilution. After washing three times, the membrane was incubated with HRP-labeled goat anti-rabbit IgG (H + L) or HRP-labeled goat anti-nouse IgG (H + L) secondary antibody (1:2,000 both; cat. nos. A0208 and A0216, respectively; both from Beyotime Institute of Biotechnology) for 2 h at room temperature, and then developed with an ECL solution (cat. no. P0018; Beyotime Institute of Biotechnology). For semi-quantitative analysis, the bands were semi-quantified using ImageJ software (v 1.53; National Institutes of Health, USA), and the data were normalized relative to the cytoplasmic control GAPDH or the nuclear control lamin B1 as the integral optical density ratio.

Reverse transcription-quantitative PCR (RT-qPCR). Total RNA was extracted from tumors or cultured HeLa cells with TRIzol® (Invitrogen; Thermo Fisher Scientific, Inc.), and its quality and quantity were assessed using NanoDrop2000c (NanoDrop Technologies; Thermo Fisher Scientific, Inc.). RNA was then reverse transcribed with random hexamers (cat. no. N8080127; Invitrogen; Thermo Fisher Scientific, Inc.) and SuperScript II kit (cat. no. 18064014; Invitrogen; Thermo Fisher Scientific, Inc.). qPCR was performed with specific primers and SYBR-Green PCR Master Mix kit (cat. no. 4368702; Applied Biosystems; Thermo Fisher Scientific, Inc.) according to the manufacturer's protocol. An 8-μl (final volume) reaction system was established, which contained 300 nM primers. The thermocycling conditions were as follows: Initial denaturation start cycle at 95˚C for 3 min, followed by 32 cycles at 95˚C for 10 sec and then 59˚C for 30 sec. The expression levels of *HIF1A* and *RelA* were calculated by the $2^{-\Delta\Delta Cq}$ method (25), normalized to that of GAPDH and converted to FC values. The following pairs of primers were used: *HIF1A* forward, 5'-GCACAGTTTGAC TTGACTGGAC-3' and reverse, 5'-TTCTTGGAGCCTGTT CTGTGG-3'; *RelA* forward, 5'-ACGAGCAGATGGTCAAGG AG-3' and reverse, 5'-CTTCCATGGTCAGTGCCTTT-3'; and GAPDH forward, 5'-GGAGCGAGATCCCTCCAAAAT-3' and reverse, 5'-GGCTGTTGTCATACTTCTCATGG-3'.

Statistical analysis. Data are expressed as the mean ± standard error of mean. Differences between two groups were compared using unpaired Student's t-test, while multiple comparisons were performed with one-way ANOVA followed by Tukey's post hoc test. In addition, multiple comparisons in two independent variables were performed with two-way ANOVA followed by Bonferroni's post hoc test. Statistical analysis was performed using SPSS v 23.0 (IBM Corp.). P<0.05 was considered to indicate a statistically significant difference.

Results

H_2 intervention reduces HeLa cell proliferation, and promotes cellular apoptosis and oxidative stress in a selective and dose-dependent manner. Firstly, the effects of H_2 treatment in HeLa cells were explored *in vitro.* As shown in Fig. 1A and B, the ratio of TUNEL-positive cells among all H_2-treated Hela cells was significantly increased compared with that
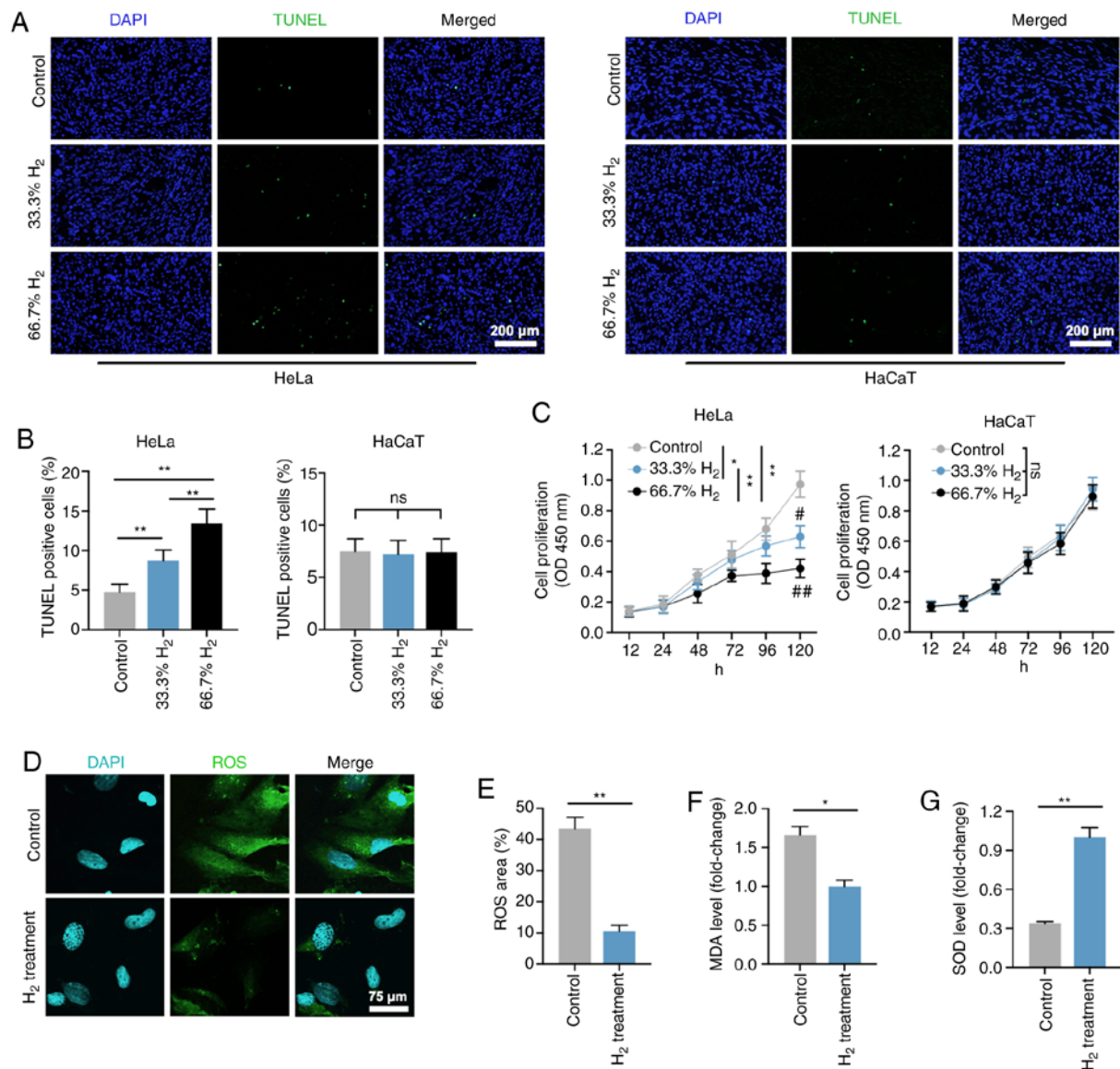
Figure 1. Decreased cell proliferation, and increased cell death and oxidative stress level in H_2-treated HeLa cervical cancer cells. (A) TUNEL staining of HeLa and HaCaT cells in the control, 33% H_2 and 66.7% H_2 groups. Furthermore, 5 μg/ml cisplatin treatment was used as a positive control (scale bar, 200 μm). (B) Statistical results of TUNEL-positive HeLa and HaCaT cells in the control, 33% H_2 and 66.7% H_2 groups (n=4 per group). **P<0.01, ns indicates no significant difference. (C) Cell proliferation curves of the control, 33% H_2 and 66.7% H_2 groups in HeLa and HaCaT cells during different time periods (n=3 per group). *P<0.05, **P<0.01 vs. indicated group, and #P<0.05, ##P<0.01 vs. control group at day 5, ns indicates no significant difference. (D) Fluorescent staining of ROS in control and 66.7% H_2-treated HeLa cells (scale bar, 75 μm). (E) Statistical results of ROS area (%) in the control and 66.7% H_2 groups (n=4 per group). **P<0.01. Statistical results of (F) malondialdehyde (MDA) and (G) superoxide dismutase (SOD) levels in the control and 66.7% H_2 treatment groups (n=5 per group). *P<0.05, **P<0.01. H_2, hydrogen; ROS, reactive oxygen species.

of the controls (P<0.01). Treatment with 66.7% H_2 markedly increased the apoptosis rate. Importantly, the increase in HeLa cell apoptotic rate induced by 5 μg/ml cisplatin treatment (IC_{50}=12 μg/ml) was consistent with the effect of 66.7% H_2 treatment. Notably, no significant differences in apoptosis rate were observed in HaCaT cells treated with or without H_2 gas. The CCK-8 assay revealed that cell proliferation was reduced after 33.3% H_2 treatment progressively, and 66.7% H_2 further decreased the proliferation of HeLa cells over time but not of HaCaT cells (Fig. 1C). In addition, the effect of time was significant associated with the cell proliferation in both Hela cells and HaCaT cells. These results suggest that H_2 has a specific concentration-dependent inhibitory effect on HeLa cells rather than on non-tumor HaCaT cells. Thus,

H_2 at a concentration of 66.7% was then used for the further experiments.

ROS are generated by ageing mitochondria due to overproduction of free radicals and reduced antioxidant defenses (26,27). The present study demonstrated that the ROS level in the H_2-treated HeLa cells was markedly reduced compared with that of the control group (P<0.01; Fig. 1D and E), which is consistent with the previously reported anti-oxidative stress activity of H_2 gas (10). In addition, the level of MDA, an indicator of lipid peroxidation, was also decreased in HeLa cells treated with H_2 (Fig. 1F), whereas an increased level in SOD, an important representative of antioxidant enzymes, was observed in the H_2 group compared with that of the controls (P<0.01; Fig. 1G). These results suggested
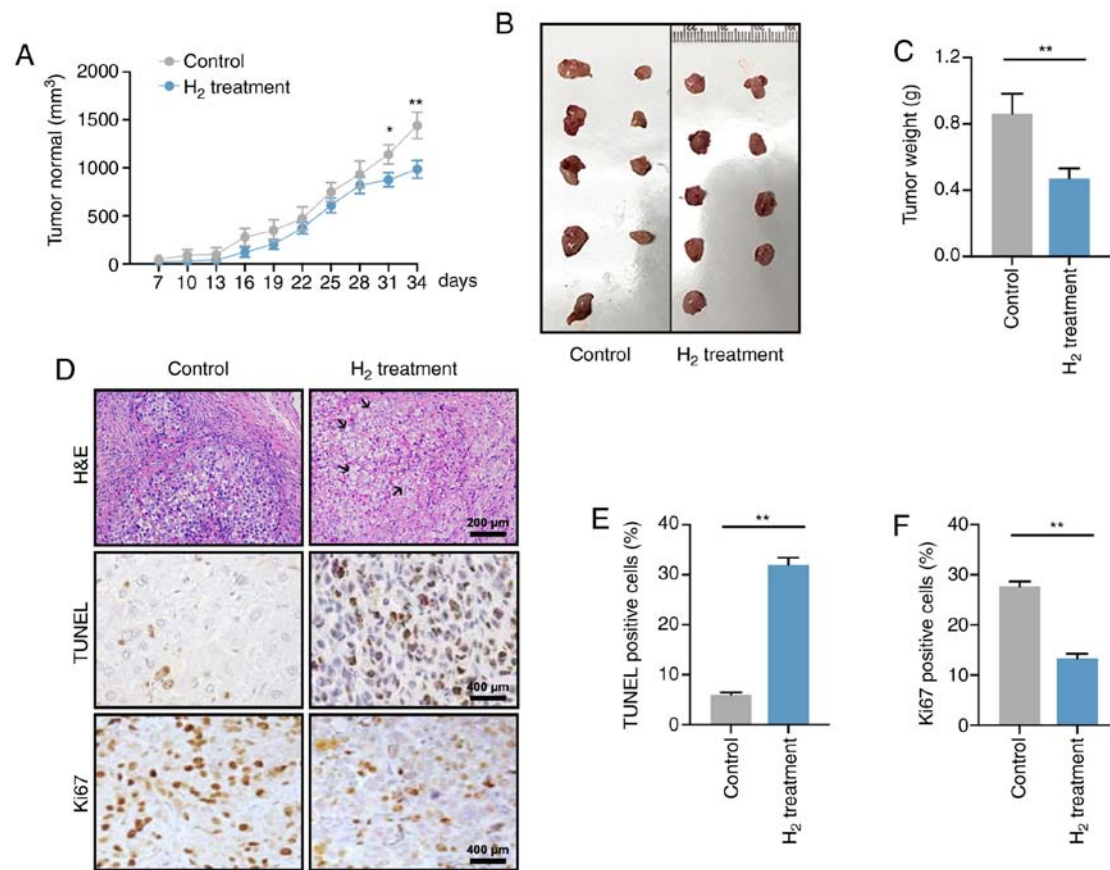
Figure 2. H_2 intervention reduces tumor growth in tumor-bearing mice. (A) Tumor volume curves from 7 to 34 days after cell injection in the control and H_2 treatment tumor-bearing groups (n=9 per group). *P<0.05, **P<0.01. (B) Images of the excised tumors in control and H_2 tumor-bearing mice. (C) Statistical results of tumor weight (units, g) in the control and H_2 groups (n=9 per group). **P<0.01. (D) Hematoxylin and eosin staining (H&E) and immunohistochemistry for TUNEL and Ki67 staining in control tumor sections or sections after treatment with H_2 (scale bar, 200 or 400 μm). Black arrows indicate nucleus fragmentation. Percentage of (E) TUNEL-positive cells or (F) Ki67-positive cells in control and H_2-treated tumors (n=5 per group). **P<0.01. H_2, hydrogen.

that H_2 intervention induced HeLa cell apoptosis, inhibited cell proliferation and reduced the oxidative stress level.

Reduced tumor growth is observed in a H_2-induced xenograft in vivo model. A total of $1x10^7$ HeLa cells were subcutaneously injected into the left armpit of nude mice, and the tumor volume was recorded every 3 days starting 7 days post-injection (Fig. 2A). At days 31 and 34, the tumor volume in mice under high H_2 environment was significantly smaller than that that in the control group (P<0.05 at day 31 and P<0.01 at day 34), which was consistent with the change in tumor weight on day 34 (P<0.01; Fig. 2B and C).

H&E staining revealed that the tumor cell death rate in the H_2 xenograft group was elevated, and was accompanied by cell swelling as well as nuclear fragmentation and disintegration (Fig. 2D; black arrows). In addition, H_2 treatment significantly increased the apoptosis rate and reduced the cell proliferation of HeLa cells (Fig. 2E and F). Taken together, these data suggested that a high-H_2 environment inhibited tumor growth in tumor-bearing mice.

Bulk RNA sequencing of H_2-treated HeLa cells and control cells. To investigate the potential mechanism by which H_2 inhibits tumor cell growth, whole-genome sequencing was performed (Fig. 3). As shown in Fig. S1A-C, 11 upregulated and 16 downregulated circular RNAs (circRNAs) were

determined in H_2-treated HeLa cells through the HiSeq4000 platform. In addition, 2 long non-coding RNAs (lncRNAs) were detected to be upregulated, while 6 lncRNAs were downregulated in H_2-treated HeLa cells (Fig. S2A-C). A total of 12 hsa-microRNAs (miRNAs or miRs) were found to be upregulated, and 2 miRNAs to be downregulated, including hsa-miR-431-5p and hsa-miR-762 (Fig. S3A-C). Importantly, mRNA sequencing revealed that 10 mRNAs were upregulated in HeLa cells subjected to H_2 treatment, and 4 mRNAs were downregulated, including *HIF1A*, *miR23B*, *miR4651* and *RelA* (Fig. 4A-C). *miR23B* and *miR4651* are non-coding RNAs, whereas *HIF1A* and *RelA* are the coding genes for HIF-1α and NF-κB p65 subunit, respectively. These results suggested that the mRNA levels of HIF-1α and NF-κB p65 subunit were reduced in H_2-treated HeLa cells compared with those of the controls.

GO enrichment analysis for HeLa cells with H_2 intervention. To further confirm the aforementioned gene regulation in H_2-treated HeLa cells, GO enrichment analysis was performed. As shown in Fig. 5A, the biological process (BP), cellular component (CC) and molecular function (MF) were analyzed. 'Translation' and 'NF-κB signaling' were the two most dominant processes in BP, and gene regulation mainly occurs in the nucleus and non-membrane-bounded organelles. MF analysis revealed that 'DNA and RNA binding' were dominant. GO
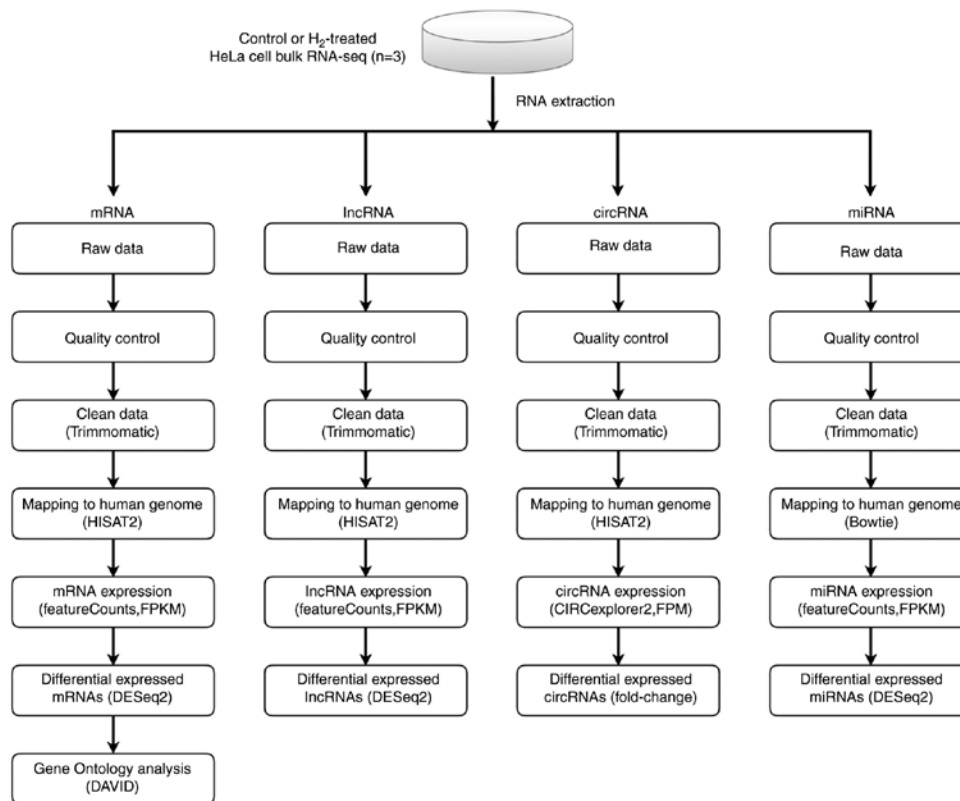
Figure 3. Scheme of whole-genome (RNA) sequencing. RNA sequencing libraries were generated from 4 mg total RNA samples isolated from control or hydrogen-treated HeLa cells using TruSeq Stranded Total RNA Library Prep kit. Sequencing was carried out on Illumina NovaSeq 6000 and HiSeq X Ten platforms. After quality control, the clean reads of circular RNA, long non-coding RNA, microRNA and mRNA were then mapped to the human genome by HISAT2 software, and the analysis was performed using an DESeq2 software. Differential expression analysis was conducted with the DESeq2 platform (n=3 per group). Gene Ontology enrichment analysis of mRNA was performed using DAVID bioinformatics tool.

enrichment scatter plot further indicated that the processes of 'NF-κB signaling', 'protein transport' and 'multicellular organismal movement' are enriched in H_2-treated HeLa cells (Fig. 5B). These results suggested that downregulation of the NF-κB signaling pathway may be an important target for H_2 intervention in HeLa cells.

HIF-1α and NF-κB p65 expression levels are downregulated in H_2-treated HeLa cells in vivo and in vitro. As the p65 subunit is a classic active type of the NF-κB family (28), the present study verified the expression levels of NF-κB p65 and HIF-1α in HeLa cells. As expected, western blot analysis demonstrated that the HIF-1α and NF-κB p65 protein levels were significantly reduced in H_2-treated HeLa cells compared with those in control HeLa cells (Fig. 6A-C). RT-qPCR analysis revealed that the mRNA expression levels of HIF-1α and NF-κB p65 (*HIF1A* and *RelA*) were elevated in HeLa cells (Fig. 6D and E).

The levels of HIF-1α and NF-κB p65 were then determined in HeLa cell-derived tumors. As shown in Fig. 6F-H, IHC demonstrated that the expression of HIF-1α and NF-κB p65 in H_2-treated HeLa tumors was significantly reduced compared with that of the controls. Furthermore, the mRNA levels *in vivo* were also investigated, and the results revealed a significant decrease in *HIF1A* and *RelA* expression in H_2-treated tumors compared with that of control tumors (Fig. 6I and J). These results indicated that the expression levels of HIF-1α and NF-κB p65 were downregulated both in HeLa cells and in HeLa tumors.

Discussion

Cervical cancer is the fourth most common type of cancer in women worldwide, and ~70% of cervical cancer cases are caused by human papilloma virus (HPV)16 and 18 infections (29). HPVs are diverse at the level of genotype and pathogenicity, and can be classified into mucosal or cutaneous according to their epithelial tropism (30). The mucosal high-risk HPV16 and HPV18 are primarily associated with squamous intraepithelial lesions, which may progress to invasive squamous cell carcinoma such as cervical cancer (31). The pathogenic effects of HPV can be avoided by preventive measures, mainly vaccination. Although the currently available immunization methods have been shown to be effective in decreasing cervical cancer, genital warts and anogenital dysplasia, the global vaccination rates remain low, and more effective alternative medical treatments are therefore needed (32).

The present study first determined the pro-apoptotic and anti-proliferative effects of H_2 treatment in HeLa cells. A H_2 concentration of 33.3% significantly increased the cell apoptosis and reduced the cell proliferation of HeLa cells but not those of non-tumor HaCaT cells. Furthermore, a high concentration of H_2 further inhibited HeLa cell proliferation and promoted cell apoptosis. These data reveal that H_2 has a dose-dependent role on cervical cancer HeLa cell suppression. Importantly, the increase in HeLa cell apoptotic rate induced by 5 μg/ml cisplatin treatment (IC_{50}=12 μg/ml) is similar to the effect of 66.7% H_2 treatment, suggesting that H_2 therapy may
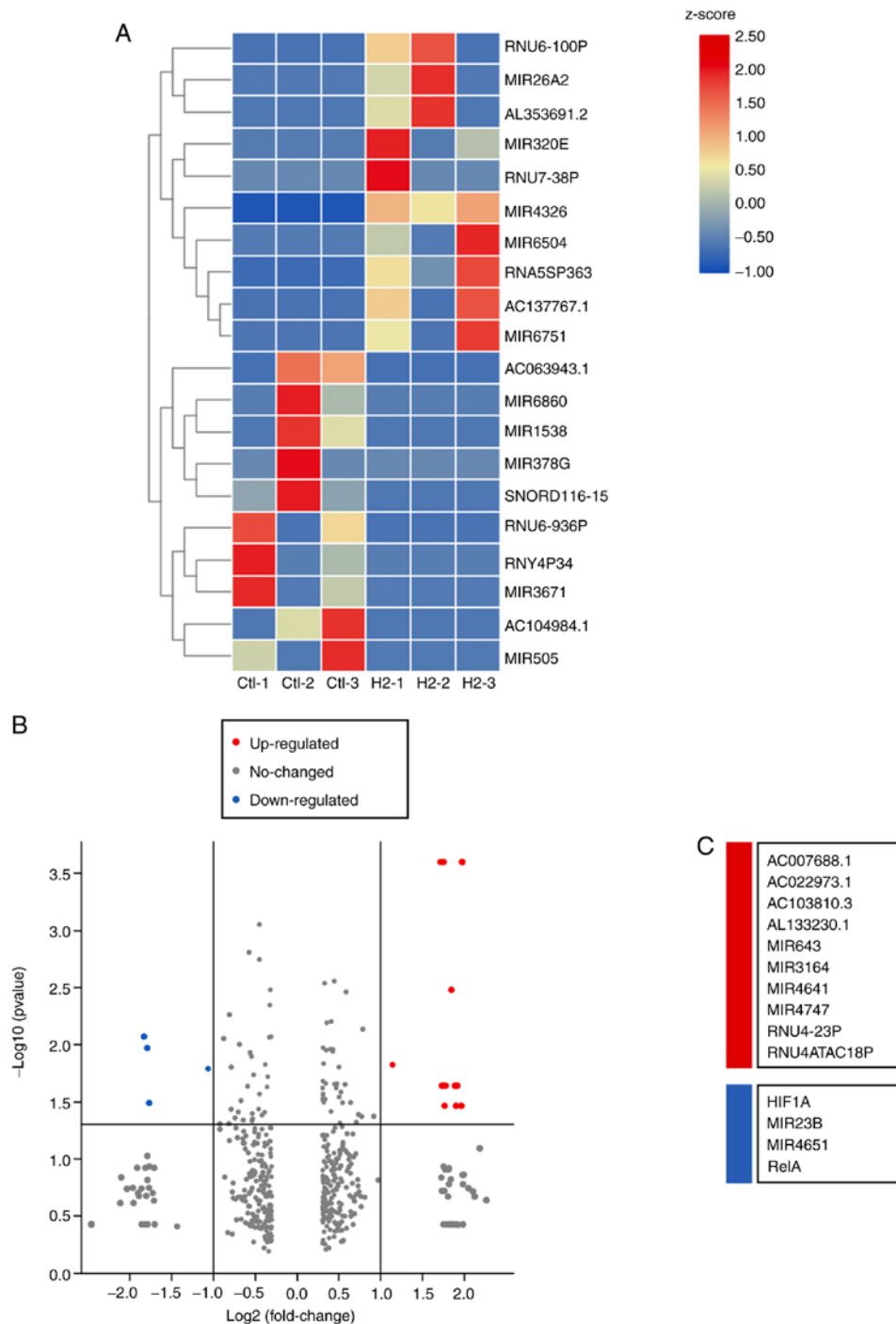
Figure 4. Highly deregulated mRNAs in HeLa cells with or without H_2 intervention. (A) A mRNA heatmap was generated based on the 10 maximum and 10 minimum FC values (n=3 per group). (B) Volcano plot for deregulated mRNAs [log2(FC) > 1 or < -1, adjusted P<0.05] between H_2 and control groups. The area above the gray horizontal solid line indicates P<0.05. (C) Upregulated mRNAs (red) and downregulated mRNAs (aqua blue) are listed. H_2, hydrogen; FC, fold-change.

be a novel therapy for cervical cancer with less toxicity and efficacy comparable to chemotherapy.

Unexpectedly, H_2 intervention reduced the oxidative stress levels, including decreased ROS and MDA concentrations, and increased SOD levels, which appeared to have the opposite effect on tumor cell suppression. The tumor inhibitory effect of H_2 was then verified in HeLa tumor-bearing mice. The tumor volume at days 31 and 34 post-injection in tumor-bearing mice with continuous H_2 treatment was significantly reduced compared with that of controls, and decreased tumor weight and cell proliferation as well as increased tumor cell apoptosis were also observed at day 34 post-injection. To explore the specific mechanisms of H_2 on HeLa cell suppression, high-throughput RNA sequencing, including cirRNA, lncRNA, miRNA and mRNA sequencing, was performed. In cervical cancer, as well as in multiple other cancer types, short, non-coding single strands of RNAs, including circRNA, lncRNA and miRNA, play a vital role, since their deregulation has been widely reported (33-35). For example, miRNA may modulate oncogenic viral gene expression, as well as the
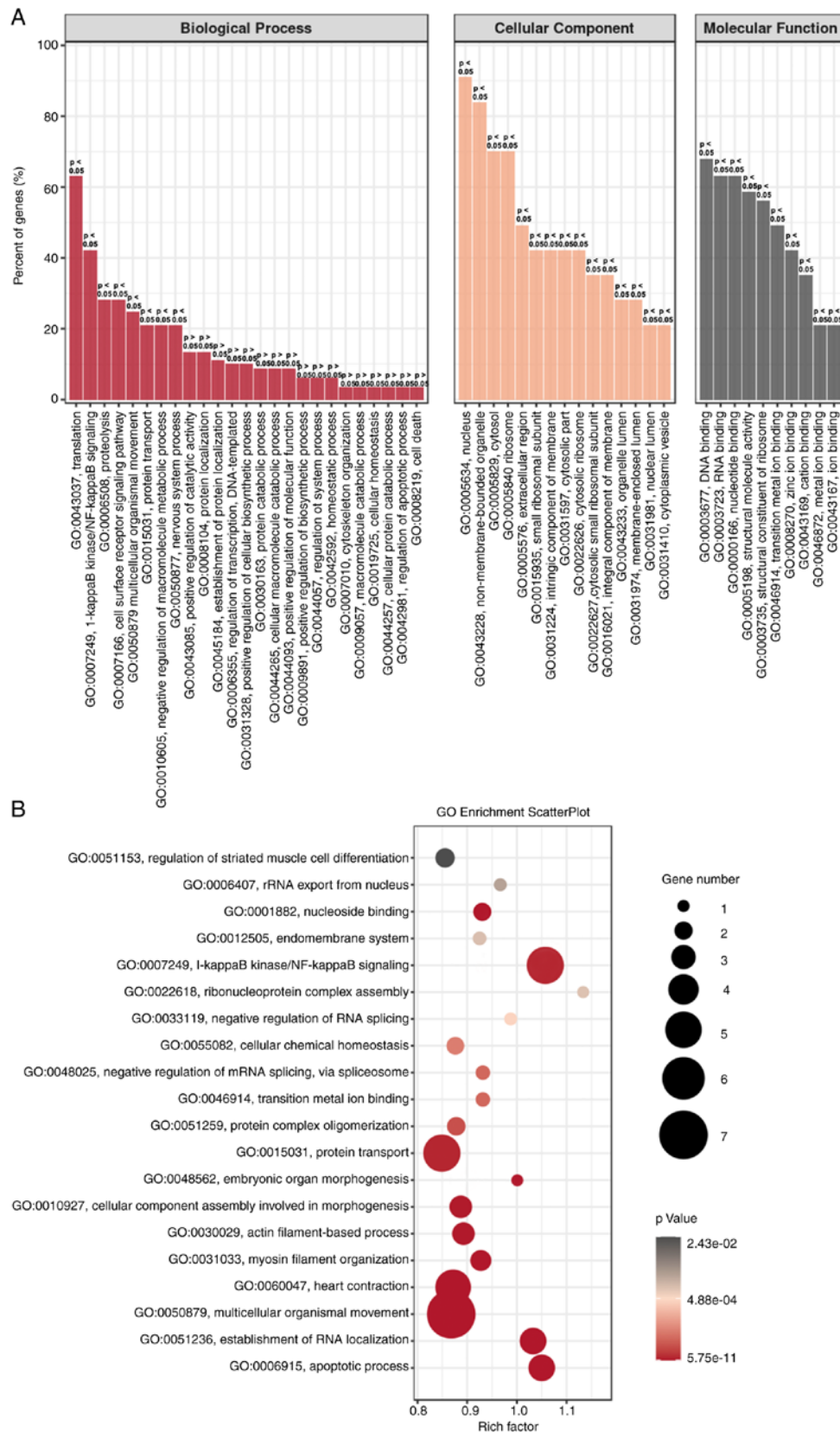
Figure 5. GO enrichment analysis of H_2-treated HeLa cells. (A) GO enrichment of BP, CC and MF analysis between H_2-treated HeLa cells and controls. (B) GO enrichment scatterplot for BP, CC and MF progress between HeLa cells with or without H_2 treatment. GO, Gene Ontology; BP, biological process, CC, cellular component; MF, molecular function; H_2, hydrogen.

gene expression of the host (36). Specifically, miRNA genes may be located at the susceptible sites in the amplified or deleted genome/regions in human tumors (37). Furthermore, as miRNAs are associated with the regulation of cell proliferation and apoptosis, changes in their expression may be responsible for proliferative disease, including cancer (38).
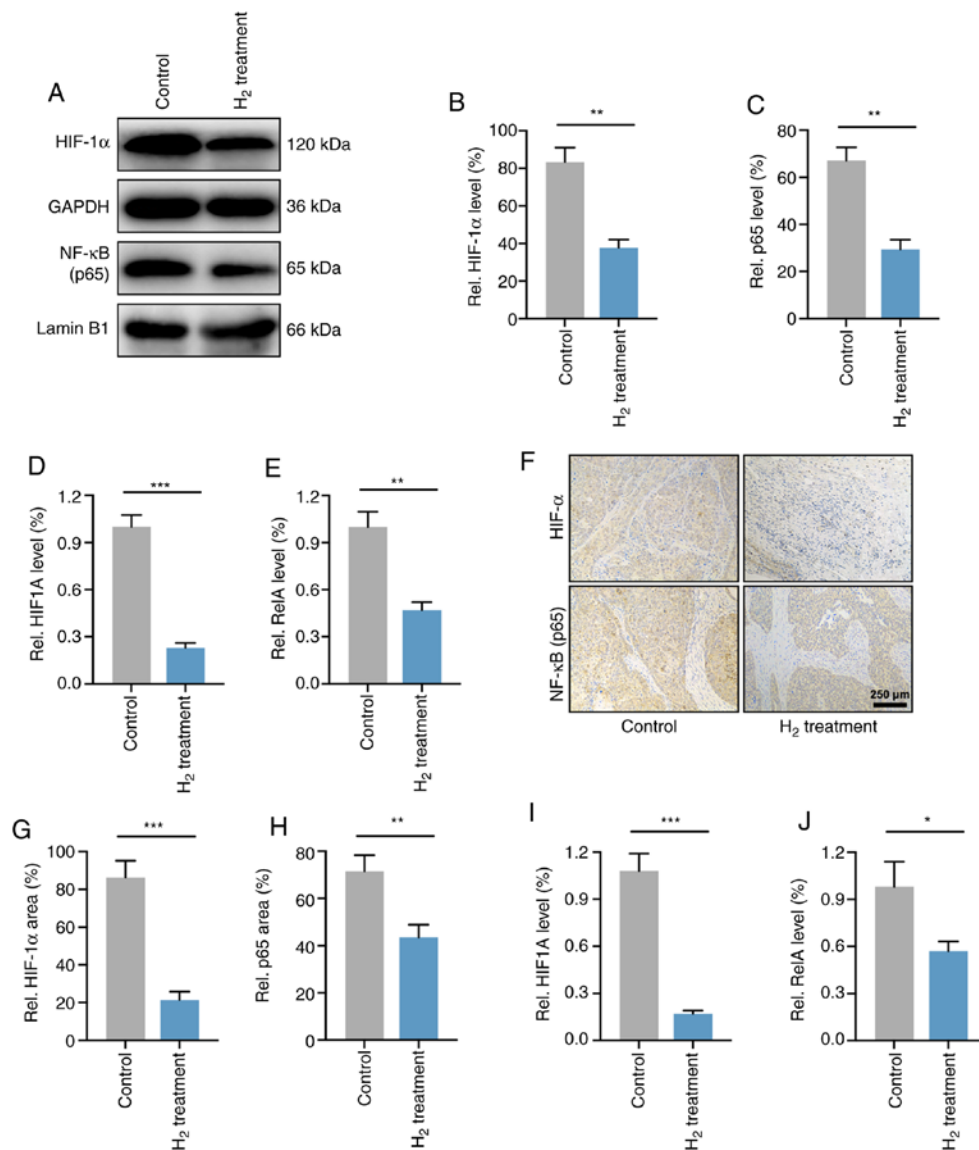
Figure 6. H_2 treatment downregulates both the gene and post-transcriptional levels of HIF-1α and NF-κB in HeLa cells and HeLa tumors. (A) Western blotting of HIF-1α and NF-κB in control and H_2-treated HeLa cells. Cytoplasmic (GAPDH) and nuclear (lamin B1) loading controls were used. (B and C) Statistical results of (B) HIF-1α and (C) NF-κB protein expression levels in HeLa cells treated with H_2 or not (n=4 per group). **$P<0.01$. RT-qPCR analysis for (D) HIF-1α mRNA (*HIF1A*) and (E) NF-κB mRNA (*RelA*) levels in control and H_2-treated HeLa cells (n=4 per group). **$P<0.01$, ***$P<0.001$. (F) Immunohistochemical analysis for determining the HIF-1α and NF-κB expression in tumor-bearing mice after H_2 intervention and their controls (scale bar, 250 μm). Percentage of positive area of (G) HIF-1α and (H) NF-κB in an *in vivo* xenograft model with or without H_2 intervention (n=9 per group). **$P<0.01$, ***$P<0.001$. (I and J) RT-qPCR analysis for (I) *HIF1A* and (J) *RelA* expression *in vivo* (n=9 per group). *$P<0.05$, ***$P<0.001$. H_2, hydrogen; HIF, hypoxia inducible factor; RT-qPCR, reverse transcription-quantitative PCR.

The present study revealed that 11 circRNAs, 2 lncRNAs and 12 miRNAs were upregulated, and 16 circRNAs, 6 lncRNAs and 2 miRNAs were downregulated in H_2-treated HeLa cells. These observations suggest that non-coding RNAs may account for the tumor inhibitory roles of H_2 on HeLa cervical cancer cells, but the specific mechanism needs to be further explored.

In addition, RNA sequencing demonstrated the changes in expression of several genes closely associated with tumor development, such as *HIF1A* and *RelA,* which encode HIF-1α and NF-κB p65 subunit, respectively. GO analysis further indicated that NF-κB signaling was involved in the inhibitory mechanism of H_2-treated HeLa cells. Declined expression of *HIF1A* and *RelA* and their translated HIF-1α and NF-κB p65 proteins was then confirmed by RT-qPCR, western blotting

and IHC both *in vitro* and *in vivo.* p65 subunit is a classic active type of the NF-κB family (28). It has been reported that NF-κB p65 is a molecular lynchpin that links chronic infection and inflammation with elevated cancer risk (39). NF-κB is persistently activated in multiple types of cancer and exerts a variety of pro-tumorigenic functions. For example, NF-κB activation in cancer cells usually leads to the elevation of anti-apoptotic genes to provide a cell survival mechanism for resisting the physiological stress that induces inflammation (40). Furthermore, NF-κB stimulates cytokines that regulate the immune response and inflammation, including TNF-α, IL-1, IL-6 and IL-8, as well as adhesion molecules, which result in the recruitment of leukocytes to inflammatory sites (28,40). In addition, NF-κB signaling was shown to modulate various other conserved cellular processes, including

cell proliferation (41,42) and apoptosis (43). H_2 intervention in HeLa cells and tumors was demonstrated to reduce both NF-κB p65 protein and mRNA levels in the RNA-sequencing and molecular biology experiments of the present study, suggesting a decrease in inflammatory response and tumor growth.

In cancer, hypoxia is considered as a vital characteristic of the tumor microenvironment that drives tumor progression (44,45). Hypoxic adaptation is largely modulated by a group of transcriptional regulators named hypoxia-inducible factors (HIFs) (46). HIF is a heterotrimeric complex consisting of an O_2-regulated α-subunit and an O_2-independent β-subunit (also called aryl hydrocarbon receptor nuclear translocator) (47). There are three HIF-α proteins recognized in humans: HIF-1α, -2α and -3α. Under normal O_2 conditions, HIF-α subunits are tightly modulated by a series of enzymes called HIF prolyl hydroxylases (PHDs). PHD is a non-heme Fe (II)- and 2-oxoglutarate-dependent dioxygenase that hydroxylates HIF-α subunits at specific prolyl residues. The hydroxylated HIF-α subunits are identified by the von-Hippel Lindau tumor-suppressor E3 ligase and degraded via the proteasome pathway (46,47). Intratumoral hypoxia induces both HIF-1 and HIF-2 activation, and overexpression of HIF-1α is strongly associated with elevated metastasis and mortality in numerous human cancer types (45,48), including cervical cancer (49). Upregulated HIF-1α in these cancer types results in a series of regulatory processes leading to tumor progression, including migration, invasion, angiogenesis, glucose metabolism and pH regulation (44,45,50,51).

The present study demonstrated that both *HIF1A* (HIF-1α gene) and HIF-1α protein levels were reduced in H_2-treated HeLa cells and HeLa tumors, which is important for elucidating the potential mechanisms of H_2 gas on cervical cancer treatment. Notably, the reduced oxidative stress observed in HeLa cells may contradict the antitumor effects of H_2. However, since ROS are essential in the stabilization of HIF that maintains the transcription of genes involved in tumor development (52), this downward trend of oxidative stress may be considered as an antitumor effect in general. Additionally, since HeLa cells are infected by HPV18 and its mechanism is associated with the regulation of oxidative stress (53), it could be hypothesized that H_2 intervention may also regulate the HPV18 genome in HeLa cells, thereby exerting a tumor-suppressor effect. Future research on this topic needs to be conducted.

The present study also has several limitations. As one of numerous cervical cancer cell lines, experiments solely on HeLa cell cells cannot determine whether all types of cervical cancer cells exhibit a consistent effect after H_2 intervention, and therefore additional cell types need to be further evaluated. Furthermore, the growth characteristics of cervical cancer cells is affected in a subcutaneous tumor model in the present study, therefore the effects of H_2 treatment are different from what would be seen in human cervical cancer. The establishment of an *in situ* cervical cancer model in follow-up experiments is therefore needed. In addition, the specific mechanism of the inhibitory effect of H_2 on HIF-1α and NF-κB (such as the regulation of the transcriptional levels of *HIF1A* and *RelA*) needs to be verified in further research. Also, the lack of negative and positive controls in this study may lead to a deviation in IHC results to a certain extent.

In conclusion, the present study suggests a novel H_2-induced tumor suppression target towards HIF-1α and NF-κB. Inhibition of HIF-1α and NF-κB reduces cervical cancer HeLa cell proliferation and oxidative stress level, and decreases tumor growth, which makes H_2 therapy a potential target in the treatment of cervical cancer.

Availability of data and materials

The datasets generated and/or analyzed during the current study are available in the Sequence Read Archive repository (https://www.ncbi.nlm.nih.gov/sra/?term=PRJNA718006),with accession number: PRJNA718006.

Authors' contributions

JC, XL, and ZJ conceived and designed the research. JC, JG, JW, LL and GC performed the *in vitro* and *in vivo* experiments. JD and ZW performed the RNA sequencing and analyzed the data. JC, JG, and XL were responsible for data analysis and writing of the manuscript. All the authors listed have approved the final manuscript.

Ethics approval and consent to participate

All animal experiments were performed in accordance with the National Institutes of Health (NIH) Guide for the Care and Use of Laboratory Animals, and were approved by the Ethics Committee for Animal Studies of Naval Medical University (approval number: 202027).

Patient consent for publication

Not applicable.

Competing interests

The authors declare that they have no competing interests.

References

1. Bray F, Ferlay J, Soerjomataram I, Siegel RL, Torre LA and Jemal A: Global cancer statistics 2018: GLOBOCAN estimates of incidence and mortality worldwide for 36 cancers in 185 countries. CA Cancer J Clin 68: 394-424, 2018.
2. Siegel RL, Miller KD and Jemal A: Cancer statistics, 2020. CA Cancer J Clin 70: 7-30, 2020.
3. Landoni F, Maneo A, Colombo A, Placa F, Milani R, Perego P, Favini G, Ferri L and Mangioni C: Randomised study of radical surgery versus radiotherapy for stage Ib-IIa cervical cancer. Lancet 350: 535-540, 1997.
4. Neeman E and Ben-Eliyahu S: Surgery and stress promote cancer metastasis: New outlooks on perioperative mediating mechanisms and immune involvement. Brain Behav Immun 30 (Suppl 1): S32-S40, 2013.

5. Hodson R: Precision medicine. Nature 537: S49, 2016.
6. Tannock IF and Hickman JA: Limits to personalized cancer medicine. N Engl J Med 375: 1289-1294, 2016.
7. Sano M, Suzuki M, Homma K, Hayashida K, Tamura T, Matsuoka T, Katsumata Y, Onuki S and Sasaki J: Promising novel therapy with hydrogen gas for emergency and critical care medicine. Acute Med Surg 5: 113-118, 2017.
8. Ge L, Yang M, Yang NN, Yin XX and Song WG: Molecular hydrogen: A preventive and therapeutic medical gas for various diseases. Oncotarget 8: 102653-102673, 2017.
9. Ohta S: Molecular hydrogen as a preventive and therapeutic medical gas: Initiation, development and potential of hydrogen medicine. Pharmacol Ther 144: 1-11, 2014.
10. Tamura T, Suzuki M, Hayashida K, Kobayashi Y, Yoshizawa J, Shibusawa T, Sano M, Hori S and Sasaki J: Hydrogen gas inhalation alleviates oxidative stress in patients with post-cardiac arrest syndrome. J Clin Biochem Nutr 67: 214-221, 2020.
11. Chen L, Chao Y, Cheng P, Li N, Zheng H and Yang Y: UPLC-QTOF/MS-based metabolomics reveals the protective mechanism of hydrogen on mice with ischemic stroke. Neurochem Res 44: 1950-1963, 2019.
12. Yang Y, Liu PY, Bao W, Chen SJ, Wu FS and Zhu PY: Hydrogen inhibits endometrial cancer growth via a ROS/NLRP3/caspase-1/GSDMD-mediated pyroptotic pathway. BMC Cancer 20: 28, 2020.
13. Wang D, Wang L, Zhang Y, Zhao Y and Chen G: Hydrogen gas inhibits lung cancer progression through targeting SMC3. Biomed Pharmacother 104: 788-797, 2018.
14. Harguindey S, Alfarouk K, Orozco JP, Hardonniere K, Stanciu D, Fais S and Devesa J: A new and integral approach to the etiopathogenesis and treatment of breast cancer based upon its hydrogen ion dynamics. Int J Mol Sci 21: 1110, 2020.
15. Chen JB, Kong XF, Lv YY, Qin SC, Sun XJ, Mu F, Lu TY and Xu KC: 'Real world survey' of hydrogen-controlled cancer: A follow-up report of 82 advanced cancer patients. Med Gas Res 9: 115-121, 2019.
16. Andrews KR, Good JM, Miller MR, Luikart G and Hohenlohe PA: Harnessing the power of RADseq for ecological and evolutionary genomics. Nat Rev Genet 17: 81-92, 2016.
17. Masters JR: HeLa cells 50 years on: The good, the bad and the ugly. Nat Rev Cancer 2: 315-319, 2002.
18. Nagaraj N, Wisniewski JR, Geiger T, Cox J, Kircher M, Kelso J, Pääbo S and Mann M: Deep proteome and transcriptome mapping of a human cancer cell line. Mol Syst Biol 7: 548, 2011.
19. Tavakolian S, Goudarzi H, Eslami G and Faghihloo E: Transcriptional regulation of epithelial to mesenchymal transition related genes by lipopolysaccharide in human cervical cancer cell line HeLa. Asian Pac J Cancer Prev 20: 2455-2461, 2019.
20. Johrens K, Lazzerini L, Barinoff J, Sehouli J and Cichon G: Mesothelin as a target for cervical cancer therapy. Arch Gynecol Obstet 299: 211-216, 2019.
21. Lin Y, Ohkawara B, Ito M, Misawa N, Miyamoto K, Takegami Y, Masuda A, Toyokuni S and Ohno K: Molecular hydrogen suppresses activated Wnt/β-catenin signaling. Sci Rep 6: 31986, 2016.
22. Kamalipooya S, Abdolmaleki P, Salemi Z, Javani Jouni F, Zafari J and Soleimani H: Simultaneous application of cisplatin and static magnetic field enhances oxidative stress in HeLa cell line. In Vitro Cell Dev Biol Anim 53: 783-790, 2017.
23. Metsalu T and Vilo J: ClustVis: A web tool for visualizing clustering of multivariate data using principal component analysis and heatmap. Nucleic Acids Res 43: W566-W570, 2015.
24. Huang da W, Sherman BT and Lempicki RA: Systematic and integrative analysis of large gene lists using DAVID bioinformatics resources. Nat Protoc 4: 44-57, 2009.
25. Rao X, Huang X, Zhou Z and Lin X: An improvement of the 2^(-delta delta CT) method for quantitative real-time polymerase chain reaction data analysis. Biostat Bioinforma Biomath 3: 71-85, 2013.
26. Finkel T and Holbrook NJ: Oxidants, oxidative stress and the biology of ageing. Nature 408: 239-247, 2000.
27. Costa V and Moradas-Ferreira P: Oxidative stress and signal transduction in Saccharomyces cerevisiae: Insights into ageing, apoptosis and diseases. Mol Aspects Med 22: 217-246, 2001.
28. DiDonato JA, Mercurio F and Karin M: NF-κB and the link between inflammation and cancer. Immunol Rev 246: 379-400, 2012.
29. Trottier H and Burchell AN: Epidemiology of mucosal human papillomavirus infection and associated diseases. Public Health Genomics 12: 291-307, 2009.
30. McBride AA: Oncogenic human papillomaviruses. Philos Trans R Soc Lond B Biol Sci 372: 20160273, 2017.
31. Viarisio D, Gissmann L and Tommasino M: Human papillomaviruses and carcinogenesis: Well-established and novel models. Curr Opin Virol 26: 56-62, 2017.
32. St Laurent J, Luckett R and Feldman S: HPV vaccination and the effects on rates of HPV-related cancers. Curr Probl Cancer 42: 493-506, 2018.
33. Tornesello ML, Faraonio R, Buonaguro L, Annunziata C, Starita N, Cerasuolo A, Pezzuto F, Tornesello AL and Buonaguro FM: The role of microRNAs, long non-coding RNAs, and circular RNAs in cervical cancer. Front Oncol 10: 150, 2020.
34. Casarotto M, Fanetti G, Guerrieri R, Palazzari E, Lupato V, Steffan A, Polesel J, Boscolo-Rizzo P and Fratta E: Beyond microRNAs: Emerging role of other non-coding RNAs in HPV-driven cancers. Cancers (Basel) 12: 1246, 2020.
35. Wen X, Liu S, Sheng J and Cui M: Recent advances in the contribution of noncoding RNAs to cisplatin resistance in cervical cancer. PeerJ 8: e9234, 2020.
36. Vojtechova Z and Tachezy R: The role of miRNAs in virus-mediated oncogenesis. Int J Mol Sci 19: 1217, 2018.
37. Calin GA and Croce CM: MicroRNA-cancer connection: The beginning of a new tale. Cancer Res 66: 7390-7394, 2006.
38. Gaur A, Jewell DA, Liang Y, Ridzon D, Moore JH, Chen C, Ambros VR and Israel MA: Characterization of microRNA expression levels and their biological correlates in human cancer cell lines. Cancer Res 67: 2456-2468, 2007.
39. Taniguchi K and Karin M: NF-κB, inflammation, immunity and cancer: Coming of age. Nat Rev Immunol 18: 309-324, 2018.
40. Hoesel B and Schmid JA: The complexity of NF-κB signaling in inflammation and cancer. Mol Cancer 12: 86, 2013.
41. Guttridge DC, Albanese C, Reuther JY, Pestell RG and Baldwin AS Jr: NF-kappaB controls cell growth and differentiation through transcriptional regulation of cyclin D1. Mol Cell Biol 19: 5785-5799, 1999.
42. La Rosa FA, Pierce JW and Sonenshein GE: Differential regulation of the c-myc oncogene promoter by the NF-kappa B rel family of transcription factors. Mol Cell Biol 14: 1039-1044, 1994.
43. Perkins ND: Achieving transcriptional specificity with NF-kappa B. Int J Biochem Cell Biol 29: 1433-1448, 1997.
44. Vaupel P and Mayer A: Hypoxia in tumors: Pathogenesis-related classification, characterization of hypoxia subtypes, and associated biological and clinical implications. Adv Exp Med Biol 812: 19-24, 2014.
45. Zhou J, Schmid T, Schnitzer S and Brune B: Tumor hypoxia and cancer progression. Cancer Lett 237: 10-21, 2006.
46. Semenza GL: Oxygen sensing, hypoxia-inducible factors, and disease pathophysiology. Annu Rev Pathol 9: 47-71, 2014.
47. Wenger RH, Stiehl DP and Camenisch G: Integration of oxygen signaling at the consensus HRE. Sci STKE 2005: re12, 2015.
48. Zhong H, De Marzo AM, Laughner E, Lim M, Hilton DA, Zagzag D, Buechler P, Isaacs WB, Semenza GL and Simons JW: Overexpression of hypoxia-inducible factor 1alpha in common human cancers and their metastases. Cancer Res 59: 5830-5835, 1999.
49. Seeber LM, Horree N, Vooijs MA, Heintz AP, van der Wall E, Verheijen RH and van Diest PJ: The role of hypoxia inducible factor-1alpha in gynecological cancer. Crit Rev Oncol Hematol 78: 173-184, 2011.
50. Keith B, Johnson RS and Simon MC: HIF1α and HIF2α: Sibling rivalry in hypoxic tumour growth and progression. Nat Rev Cancer 12: 9-22, 2011.
51. Scholz CC and Taylor CT: Targeting the HIF pathway in inflammation and immunity. Curr Opin Pharmacol 13: 646-653, 2013.
52. Hervouet E, Cizkova A, Demont J, Vojtiskova A, Pecina P, Franssen-van Hal NL, Keijer J, Simonnet H, Ivanek R, Kmoch S, et al: HIF and reactive oxygen species regulate oxidative phosphorylation in cancer. Carcinogenesis 29: 1528-1537, 2008.
53. Hao Y, Yan Z, Zhang A, Hu S, Wang N, Luo XG, Ma W, Zhang TC and He H: IL-6/STAT3 mediates the HPV18 E6/E7 stimulated upregulation of MALAT1 gene in cervical cancer HeLa cells. Virus Res 281: 197907, 2020.